

# Self-action of continuous laser radiation and Pearcey diffraction in a water suspension with light-absorbing particles

**Angelsky, O. V.; Bekshaev, A. Ya.; Maksimyak, P. P.; Maksimyak, A. P.; Hanson, Steen Grüner; Zenkova, C. Yu.**

*Published in:*
Optics Express

*Link to article, DOI:*
10.1364/OE.22.002267

*Publication date:*
2014

*Document Version*
Publisher's PDF, also known as Version of record

# Self-action of continuous laser radiation and Pearcey diffraction in a water suspension with light-absorbing particles

**O. V. Angelsky,[1]* A. Ya. Bekshaev,[2] P. P. Maksimyak,[1] A. P. Maksimyak,[1] S. G. Hanson,[3] and C. Yu. Zenkova[4]**

[1]*Correlation Optics Department, Chernivtsi National University, 2, Kotsyubinsky Str., Chernivtsi 58012, Ukraine*
[2]*Physical Department, Odessa I.I. Mechnikov National University, Dvorianska 2, Odessa 65082, Ukraine*
[3]*DTU Fotonik, Department of Photonics Engineering, DK-4000 Roskilde, Denmark*
[4]*Department of Optics and Spectroscopy, Chernivtsi National University, 2, Kotsyubinsky Str., Chernivtsi 58012, Ukraine*
**angelsky@itf.cv.ua*

**Abstract**: Water suspension of light-absorbing nano-sized particles is an example of a medium in which non-linear effects are present at moderate light intensities favorable for optical treatment of organic and biological objects. We study experimentally the phenomena emerging in a thin layer of such a medium under the action of inhomogeneous light field formed due to the Pearcey diffraction pattern near a microlens focus. In this high-gradient field, the light energy absorbed by the particles induces inhomogeneous distribution of the medium refraction index, which results in observable self-diffraction of the incident light, here being strongly sensitive to the medium position with respect to the focus. This technique, based on the complex spatial structure of both the incident and the diffracted fields, can be employed for the detection and measurement of weak non-linearities.



OCIS codes: (260.2160) Energy transfer; (260.5430) Polarization; (350.4855) Optical tweezers or optical manipulation; (350.4990) Particles.

## References and links

1. A. Ashkin, "Acceleration and trapping of particles by radiation pressure," Phys. Rev. Lett. **24**(4), 156–159 (1970).
2. A. Ashkin and J. P. Gordon, "Stability of radiation-pressure particle traps: an optical Earnshaw theorem," Opt. Lett. **8**(10), 511–513 (1983).
3. A. Ashkin, J. M. Dziedzic, J. E. Bjorkholm, and S. Chu, "Observation of a single-beam gradient force optical trap for dielectric particles," Opt. Lett. **11**(5), 288–290 (1986).
4. D. G. Grier, "A revolution in optical manipulation," Nature **424**(6950), 810–816 (2003).
5. M. Dienerowitz, M. Mazilu, and K. Dholakia, "Optical manipulation of nanoparticles: a review," J. Nanophoton. **2**(1), 021875 (2008).
6. T. A. Nieminen, J. Higuet, G. Knoner, V. L. Y. Loke, S. Parkin, W. Singer, N. R. Heckenberg, and H. Rubinsztein-Dunlop, "Optically driven micromachines: progress and prospects," Proc. SPIE **6038**, 237–245 (2006).
7. V. G. Shvedov, A. S. Desyatnikov, A. V. Rode, W. Krolikowski, and Y. S. Kivshar, "Optical guiding of absorbing nanoclusters in air," Opt. Express **17**(7), 5743–5757 (2009).
8. A. S. Desyatnikov, V. G. Shvedov, A. V. Rode, W. Krolikowski, and Y. S. Kivshar, "Photophoretic manipulation of absorbing aerosol particles with vortex beams: theory versus experiment," Opt. Express **17**(10), 8201–8211 (2009).
9. A. Y. Bekshaev, "Subwavelength particles in an inhomogeneous light field: Optical forces associated with the spin and orbital energy flows," J. Opt. **15**(4), 044004 (2013).
10. A. Y. Bekshaev, K. Bliokh, and M. Soskin, "Internal flows and energy circulation in light beams," J. Opt. **13**(5), 053001 (2011).
11. A. Y. Bekshaev, O. V. Angelsky, S. G. Hanson, and C. Y. Zenkova, "Scattering of inhomogeneous circularly polarized optical field and mechanical manifestation of the internal energy flows," Phys. Rev. A **86**(2), 023847 (2012).

#199166 - $15.00 USD Received 8 Oct 2013; revised 30 Dec 2013; accepted 6 Jan 2014; published 28 Jan 2014

12. Y. Q. Zhao, J. S. Edgar, G. D. M. Jeffries, D. McGloin, and D. T. Chiu, "Spin-to-orbital angular momentum conversion in a strongly focused optical beam," Phys. Rev. Lett. **99**(7), 073901 (2007).
13. A. T. O'Neil, I. MacVicar, L. Allen, and M. J. Padgett, "Intrinsic and extrinsic nature of the orbital angular momentum of a light beam," Phys. Rev. Lett. **88**(5), 053601 (2002).
14. J. E. Curtis and D. G. Grier, "Structure of optical vortices," Phys. Rev. Lett. **90**(13), 133901 (2003).
15. V. Garcés-Chávez, D. McGloin, M. J. Padgett, W. Dultz, H. Schmitzer, and K. Dholakia, "Observation of the transfer of the local angular momentum density of a multiringed light beam to an optically trapped particle," Phys. Rev. Lett. **91**(9), 093602 (2003).
16. O. V. Angelsky, A. Ya. Bekshaev, P. P. Maksimyak, A. P. Maksimyak, S. G. Hanson, and C. Yu. Zenkova, "Orbital rotation without orbital angular momentum: mechanical action of the spin part of the internal energy flow in light beams," Opt. Express **20**(4), 3563–3571 (2012).
17. O. V. Angelsky, A. Ya. Bekshaev, P. P. Maksimyak, A. P. Maksimyak, I. I. Mokhun, S. G. Hanson, C. Yu. Zenkova, and A. V. Tyurin, "Circular motion of particles suspended in a Gaussian beam with circular polarization validates the spin part of the internal energy flow," Opt. Express **20**(10), 11351–11356 (2012).
18. Y. Wada, S. Totoki, M. Watanabe, N. Moriya, Y. Tsunazawa, and H. Shimaoka, "Nanoparticle size analysis with relaxation of induced grating by dielectrophoresis," Opt. Express **14**(12), 5755–5764 (2006).
19. O. V. Angelsky, A. Ya. Bekshaev, P. P. Maksimyak, A. P. Maksimyak, S. G. Hanson, and C. Yu. Zenkova, "Self-diffraction of continuous laser radiation in a disperse medium with absorbing particles," Opt. Express **21**(7), 8922–8938 (2013).
20. D. N. Auston, D. J. Bradley, A. J. Campillo, K. B. Eisenthal, E. P. Ippen, D. von der Linde, C. V. Shank, and S. L. Shapiro, Ultrashort Light Pulses: Picosecond Technique and Applications (Springer-Verlag, 1977).
21. S. A. Akhmanov, V. A. Vysloukh, and A. S. Chirkin, "Self-action of wave packets in a nonlinear medium and femtosecond laser pulse generation," Sov. Phys. Usp. **29**(7), 642–647 (1986).
22. V. L. Vinetskiĭ, N. V. Kukhtarev, S. G. Odulov, and M. S. Soskin, "Dynamic self-diffraction of coherent light beams," Sov. Phys. Usp. **22**(9), 742–756 (1979).
23. S. A. Akhmanov, A. P. Sukhorukov, and R. V. Khokhlov, "Self-focusing and diffraction of light in a nonlinear medium," Sov. Phys. Usp. **10**(5), 609–636 (1968).
24. J.-G. Tian, C. Zhang, and G. Zhang, "The origin of optical nonlinearities of chinese tea," Optik (Stuttg.) **90**, 1–4 (1992).
25. J.-G. Tian, C. Zhang, G. Zhang, and J. Li, "Position dispersion and optical limiting resulting from thermally induced nonlinearities in Chinese tea liquid," Appl. Opt. **32**(33), 6628–6632 (1993).
26. K.-E. Peiponen and R. Uma Maheswari, C. Gu, and T. Jaaskelainen, "Heat-induced transient optical effects in chinese tea," Optik (Stuttg.) **93**, 167–169 (1993).
27. H.-J. Zhang, J.-H. Dai, P.-Y. Wang, and L.-A. Wu, "Self-focusing and self-trapping in new types of Kerr media with large nonlinearities," Opt. Lett. **14**(13), 695–696 (1989).
28. M. Sheik-bahae, A. A. Said, and E. W. Van Stryland, "High-sensitivity, single-beam $n_2$ measurements," Opt. Lett. **14**(17), 955–957 (1989).
29. J. F. Nye, "Evolution from Fraunhofer to a Pearcey diffraction pattern," J. Opt. A, Pure Appl. Opt. **5**(5), 495–502 (2003).
30. J. F. Nye, "From Airy rings to the elliptic umbilic diffraction catastrophe," J. Opt. A, Pure Appl. Opt. **5**(5), 503–510 (2003).
31. T. Pearcey, "The structure of an electromagnetic field in the neighbourhood of a cusp of a caustic," Philos. Mag. **37**, 311–317 (1946).
32. M. Born and E. Wolf, Principles of Optics (New York, Pergamon Press., 1999).
33. S. M. Rytov, Y. A. Kravtsov, and V. I. Tatarskii, Principles of Statistical Radiophysics 3: Elements of Random Fields (Springer-Verlag, 1989).
34. P. Gerstner, J. Paltakari, and P. A. C. Gane, "Measurement and modelling of heat transfer in paper coating structures," http://www.tappi.org/Downloads/Conference-Papers/2008/08ADV/08adv26.aspx.
35. S. H. Simpson and S. Hanna, "Orbital motion of optically trapped particles in Laguerre-Gaussian beams," J. Opt. Soc. Am. A **27**(9), 2061–2071 (2010).
36. N. V. Malai, "Effect of motion of the medium on the photophoresis of hot hydrosol particles," Fluid Dyn. **41**(6), 984–991 (2006).
37. C. Y. Soong, W. K. Li, C. H. Liu, and P. Y. Tzeng, "Theoretical analysis for photophoresis of a microscale hydrophobic particle in liquids," Opt. Express **18**(3), 2168–2182 (2010).

## 1. Introduction

During the past decades, the specific behavior of small particles under the action of light has become a powerful and efficient tool in fundamental and applied optical research. Since the pioneering work by Ashkin et al [1–3], light-induced mechanical effects have been widely used for trapping, transportation, orientation and localization of micro-particles (see, e.g., Refs [4–8].), as well as for the study of fine structure of light fields [9–17]. Among various further applications, the use of ensembles of suspended optically-driven micro- and

#199166 - $15.00 USD Received 8 Oct 2013; revised 30 Dec 2013; accepted 6 Jan 2014; published 28 Jan 2014

nanoparticles has recently been proposed as a means for the control and regulation of light propagation [18,19].

In absorptive media, propagation of inhomogeneous optical radiation induces non-uniform distributions of temperature and, consequently, of many associated optical constants. The corresponding effects are coupled with self-diffraction, self-focusing and emergence of shock waves. Usually, such self-action phenomena accompany the propagation of short powerful laser pulses [20–23] where, due to high density of the absorbed energy, the medium may be damaged. This is detrimental, for example, in the study of organic and biological objects.

Continuous laser radiation of moderate power can also produce a temperature gradient but normally it is insufficient to generate noticeable non-linear self-action of the optical field. Relatively large thermal non-linearity was observed in the ethanol solutions of the Chinese tea liquid [24–26] where the self-induced lens effect was attributed to strong absorption of the He-Ne laser radiation by molecules of chlorophyll and similar herbal dyes [27]. However, in such solutions the non-linear effects were only observable in considerably thick samples (~1 mm).

Recently, we have demonstrated the possibility of extremely high thermal inhomogeneity in a dielectric medium containing suspended absorbing particles [19]. In such systems, remarkable non-linear phenomena may occur within micron-size volumes in the sparing regime preserving integrity of the medium and its constituents. This fact can be used in micro- and nanotechnologies as well as in diagnostics and selective treatment of biological objects. The present work is devoted to the study and realization of the corresponding possibilities.

Usual ways for detection and measurement of weak nonlinearities are based on the well-known Z scan method [28] in which the sample is placed within a focused Gaussian beam and takes different longitudinal positions near the focal point. Then the quantitative characteristics of the non-linearity are derived from the additional focusing (or defocusing) of the beam which takes place in the sample [23–25]. However, the "strength" of the self-induced inhomogeneity (e.g., the refractive index gradient) inversely depends on the near-focus beam size which cannot be arbitrary small, and this limits the method sensitivity. This limitation can be overcome if the incident field inhomogeneity appears not only due to focusing but also due to additional modulations, e.g. caused by two-wave interference. Emergence of fine periodic structures is especially favorable for the study of weak non-linear effects as it provokes the suitably observable self-diffraction phenomena [19].

In this work, we continue the exploration of the non-linear effects in a disperse medium under the action of a strongly inhomogeneous optical field with moderate power. In view of the above paragraph, the next step is to employ an incident field with a controllable speckle pattern, regular both in the transverse and longitudinal directions. Such situations occur in the coherent optical field formed after a collimated beam passes a thick cylindrical lens. Due to strong aberrations, this focused field is characterized by the special features [29,30]: (i) the intensity distribution is bounded by the caustic surface and (ii) the amplitude and phase distributions contain the well-developed and regular system of bright and dark spots accompanied by the phase singularities, known as the Pearcey diffraction pattern [31].

The methods and background of this work represent a further development of the Z scan method [24,25,28] and the approach employed for investigation of the self-diffraction processes of the two-beam interference field in the same disperse media [19]. The disperse medium (dielectric liquid + suspended particles) is initially characterized by a homogeneous distribution of absorbing particles. Exposure of this medium to an optical field with a spatially inhomogeneous intensity distribution results in inhomogeneous heating, which, in turn, makes the medium refraction index coordinate-dependent. If the disperse medium is situated close to the focal plane of the cylindrical lens, additional modulations of the refraction index in the medium due to the light absorption by the particles becomes strong enough to cause a perturbation of the propagating light beam. As a result, this will induce

#199166 - $15.00 USD Received 8 Oct 2013; revised 30 Dec 2013; accepted 6 Jan 2014; published 28 Jan 2014

self-diffraction processes that manifest themselves via the intensity redistribution in the beam leaving the medium. We have performed computer simulation and experimental modeling of this effect for different positions of the sample with respect to the lens focus, and confronting the simulation and experimental data served to measure the non-linear characteristics of the medium.

## 2. The Pearcey diffraction pattern

The geometrical conditions of the problem are illustrated by Fig. 1. The action of the cylindrical lens is considered as a passage through a phase transparency with a transmission function $\exp\left[ik(m-1)h(x)\right]$ where $k=2\pi/\lambda$ ($\lambda$ is the radiation wavelength in vacuum), $m$ is the lens refraction index, and $h(x)=\sqrt{r^2-x^2}$ is the lens profile function with $r$ being the radius of the lens cylindrical surface. For calculation of the field amplitude after the lens we employ the two-dimensional scalar Rayleigh – Sommerfeld diffraction integral [32]

$$U(\xi,z)=\frac{z}{\sqrt{i\lambda}}\int\frac{F(x)}{R^{3/2}(x,z,\xi)}\exp\left\{ik\left[R(x,z,\xi)+(m-1)h(x)\right]\right\}dx \qquad (1)$$

Here $R(x,z,\xi)=\sqrt{(z-r)^2+(x-\xi)^2}$ is the distance from a point in the lens output plane (P) with the transverse coordinate $x$ to a point in the observation plane (C) with the transverse coordinate $\xi$, $z$ is the distance between the aperture plane and the observation plane (plane $z$ = 0 coincides with the flat input face of the lens as shown in Fig. 1). The input field is assumed to be a plane wave with unit amplitude, then the aperture function $F(x)$ can be approximated by the rectangular distribution which equals 1 if $|x|<r/m$ and vanishes for other $x$ because of the total internal reflection in the lens.

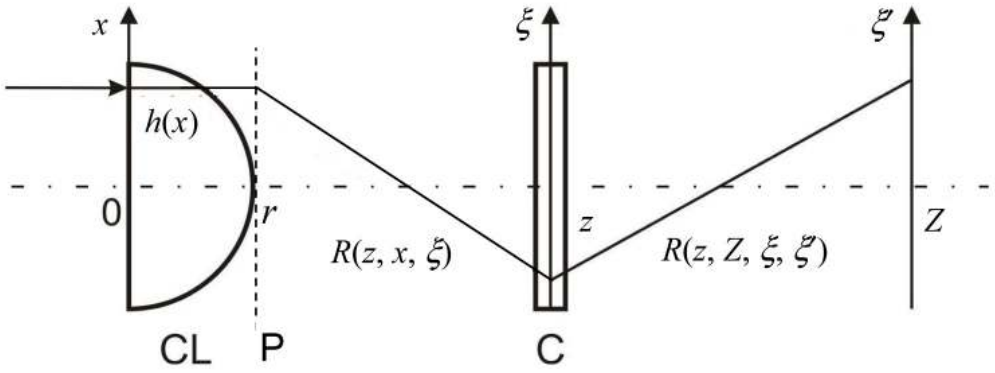


Fig. 1. Setup for calculation of the optical field focused by the cylindrical lens CL in the cell C with the disperse medium.

In contrast to the Kirchhoff integral [32,33], Eq. (1) is applicable to field calculations at small distances between the pupil plane ($z = r$) and the observation plane. Figure 2 shows the calculated intensity distribution $I(z,\xi)$ in the region $z > r$ for a lens aperture 20 μm and the cylindrical surface radius $r=10$ μm together with the results experimentally observed where the cylindrical lens was formed by a segment of an optical fiber with appropriate radius and refraction index $m=1.528$; the radiation wavelength is $\lambda$ = 445 nm. Because of the high spherical aberrations of the lens whose action is illustrated in Fig. 2, its geometric-optics focus does not coincide with the point of maximal energy concentration. Due to the better experimental localizability, the latter is a suitable reference point and from now on we will,

#199166 - $15.00 USD Received 8 Oct 2013; revised 30 Dec 2013; accepted 6 Jan 2014; published 28 Jan 2014

conventionally, apply the term 'focal plane' to the transverse plane containing the single axial brightest spot. According to Fig. 2a, this plane corresponds to $z = 28\,\mu\text{m}$. Figure 2b represents a fragment of the intensity distribution observed in the near-focal region with the help of an oblique photodetector facilitating the visualization of the longitudinal intensity distribution. It clearly reproduces not only caustics but many minor details of the calculated Pearcey pattern.

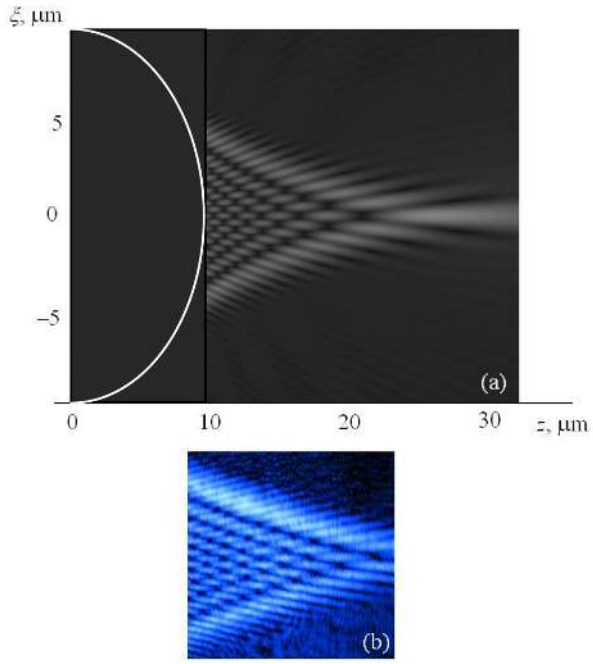


Fig. 2. (a) Intensity distribution after the cylindrical lens calculated via Eq. (1) for $r$ = 10 μm and $\lambda$ = 445 nm, solid line is the lens contour; (b) experimental intensity pattern observed in the near-focus region.

### 3. Influence of the disperse medium near the lens focus

The presence of the cell C with the dispersed medium leads to modification of the standard Pearcey pattern of Fig. 2 in any plane located behind the cell (see Fig. 1). Let the cell be placed in a certain plane $z$ near the focus and the plane of observation be situated at the distance $Z$ from the cylindrical lens, $Z > z$. In this plane, the field amplitude distribution $U(\xi', z, Z)$ distorted due to interaction with the disperse medium can be calculated with the help of the modified diffraction integral (1),

$$U(\xi', z, Z) = \frac{Z - z}{\sqrt{i\lambda}} \int \frac{U(\xi, z)}{R^{3/2}(Z, z, \xi, \xi')} \exp\left(-\frac{1}{2}\alpha d\right) \times \exp\left\{-i\left[k\,R(Z, z, \xi, \xi') + k\,\Delta n(\xi, z) d\right]\right\} d\xi, \tag{2}$$

where $U(\xi, z)$ is the incident beam amplitude in the cell plane, $R(Z, z, \xi, \xi') = \sqrt{(Z - z)^2 + (\xi' - \xi)^2}$ is the distance between the point with coordinates $(\xi, z)$ in the cell plane and the point of observation with coordinates $(\xi', Z)$, $\Delta n(\xi, z)$ is the field-induced modulation of the disperse medium refraction index, $\alpha$ is the intensity-independent

#199166 - $15.00 USD Received 8 Oct 2013; revised 30 Dec 2013; accepted 6 Jan 2014; published 28 Jan 2014

absorption coefficient and $d$ is the thickness of the disperse medium in the cell. In Eq. (2) we suppose the medium layer to be thin enough so that it can be treated as a thin phase transparency with complex amplitude transmission function $\exp\left[-(1/2)\alpha d + i\,k\Delta n(\xi,z)d\right]$.

**Table 1. Values of the disperse medium parameters used in the calculation of the radiation-induced refraction index modification (Eqs. (3) and (4)).**

| | | |
|---|---|---|
| 1 | Mean size of the pigment particles | 0.2 μm |
| 2 | Concentration of the pigment particles | 0.4 g·cm$^{-3}$ |
| 3 | Complex refraction index of the particle coating | 1.82 + 0.74i |
| 4 | Refraction index of the matrix medium (water) | 1.33 |
| 5 | Absorption coefficient of the medium | $7\cdot10^{2}$ cm$^{-1}$ |
| 6 | Cell thickness | 10 μm ($\alpha d$ = 0.7) |
| 7 | Radiation wavelength | 0.445 μm ($k = 2\pi/\lambda = 1.41\cdot10^{5}$ cm$^{-1}$) |
| 8 | Refractive index temperature coefficient | $(dn/dT) = -0.8\cdot10^{-4}$ K$^{-1}$ |
| 9 | Specific heat capacity (water) | 4.2 kJ·kg$^{-1}$·K$^{-1}$ |
| 10 | Mass density (water) | $10^{3}$ kg·m$^{-3}$ |

The absorption coefficient $\alpha$ is an effective medium characteristic determined by averaging the light absorption in individual particles, taking into account their distribution and concentration. The pigment particles used in our experiments are close to spherical with mean radius $a = 0.1\,\mu\text{m}$ and contain ~20 nm absorptive coating of carbon-based resin. The complex refraction index of the coating is assumed to be close to that of the atmospheric soot [34]. The parameters of the particles and of the disperse medium used in the experiment are specified in Table 1.

For evaluation of Eq. (2), the key quantity is $\Delta n(z,\xi)$. In the first approximation we assume that it is determined completely by the incident field, and that the prevailing mechanism for the refraction index modulation is associated with inhomogeneous heating of the medium due to the light energy absorption [19]. In view of the small thickness of the medium layer compared with the longitudinal scale of the near-focus Pearcey pattern, all points of the medium with the same transverse coordinates experience practically the same field-induced action. In such conditions, the density of the additional energy accumulated in the point $(\xi,z)$ (i.e. 'stationary absorbed energy' [19]) within the cell equals

$$q(\xi,z) = \alpha\eta I(\xi,z)\exp(-\alpha z), \tag{3}$$

where $n_0$ is the basic (zero-intensity) value of the medium refraction index, $I(\xi,z)$ is the intensity (energy flow density) in the incident light field: if amplitude (1) characterizes the electric field of the electromagnetic wave, $I(z,\xi) = (cn_0/8\pi)\left|U(z,\xi)\right|^2$ in the Gaussian system of units. In Eq. (3), $\eta$ is the efficiency coefficient, with the dimension of time, whose meaning is close to the time of thermal relaxation [25]. It characterizes the stationary state of inhomogeneous energy accumulation which depends on interplay between the rates of light energy absorption in high-intensity regions and of the absorbed energy leakage to low intensity regions. Its exact definition relies on the heat conductivity, diffusion and convection arguments but here its introduction enables us to link the spatial distribution of the accumulated energy with the incident beam intensity distribution [19]. We do not specify it more exactly because, in calculations, $\eta$ was considered as a fitting parameter determined from the condition of the best agreement with the experimental data (see below).

Corresponding variation of the refraction index can be expressed in the form

#199166 - $15.00 USD Received 8 Oct 2013; revised 30 Dec 2013; accepted 6 Jan 2014; published 28 Jan 2014

$$\Delta n = \Delta n(\xi, z) = \left(\frac{dn}{dT}\right)\frac{q(\xi, z)}{C\rho} \tag{4}$$

where $(dn/dT)$ is the refractive index temperature coefficient, $C$ is the specific heat capacity (per unit mass of the medium) and $\rho$ is the medium mass density; for simplicity, here we suppose $\Delta n$ to be proportional to $q$ thereby neglecting possible distortion of the absorbed energy distribution due to the heat conductivity. Combining Eqs. (3) and (4) determines the spatial distribution of the induced medium inhomogeneity.

According to these equations, the field-induced non-uniform heating only affects the real refraction index thus forming a phase grating. Additionally, due to the gradient optical force [2,9,35] and the photophoresis [7,8,36,37], the suspended particles may concentrate near the intensity minima which contributes to the creation of an amplitude inhomogeneity. However, direct estimates [19] show that at moderate light power, compatible with the medium stability (~40 mW to prevent the water boiling and cavitation effects), variation of the particles' concentration does not exceed 5% and in the actual conditions, influence of the amplitude inhomogeneity is negligible. This permits us to restrict the analysis to the case of a homogeneous particle distribution.

A schematic drawing of the experimental setup is presented in Fig. 3. As a radiation source, the semiconductor laser XJ-A140 was used with wavelength $\lambda$ = 445 nm and controllable power ≤ 0.3 W. The laser radiation is linearly polarized in the plane orthogonal to the figure plane, which coincides with the focusing plane of the cylindrical lens CL and justifies the scalar approximation of Eqs. (1) and (2). Telescope T consisting of two micro-objectives with a pinhole diaphragm in the common focus forms a parallel beam of 10 mm in diameter. Further, the beam is focused by the lens CL onto the silica cell C containing the medium (water) with suspended particles. The lens is made of glass with refraction index $m$ = 1.52 in the shape of a cylindrical segment enclosed between the plane input face and the cylindrical surface of radius $r$ = 1.8 mm; the lens size along the vertical ($x$) direction equals 3.6 mm and along the $y$-direction 8 mm. The use of the macroscopic arrangement (in contrast to the micron-size lens discussed in Section 2) is not of principal importance and was motivated by convenience of the cell manipulations. However, in this arrangement we could not measure the 3D diffraction pattern directly but the image of Fig. 2b can still be applied in view of the spatial similarity laws regulating the Pearcey pattern [29]. The lens focus defined as the position of the highest light concentration near the system axis (see Section 2) is located at a distance of $f$ = 5 mm from the lens input plane; the plane of observation is situated at $Z$ = 15 mm (10 mm behind the focus). The cell walls are of thickness 0.5 mm and enclose a 10 μm layer of the disperse medium. During normal working conditions, the light power reaching the cell is approximately 50 mW.

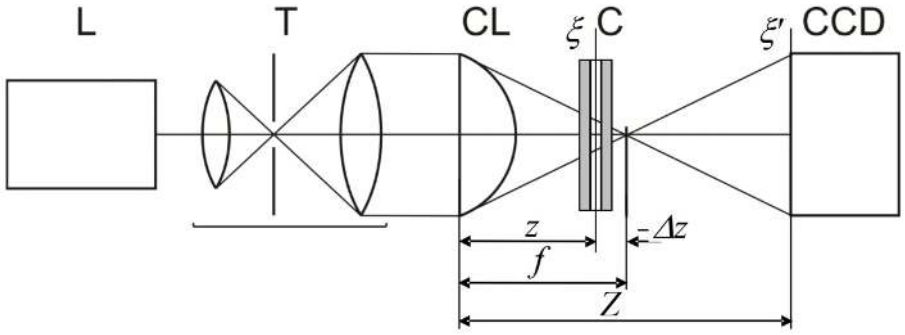


Fig. 3. Optical scheme of the setup for investigation of the focused beam transformation in the disperse medium (explanations in the text).

#199166 - $15.00 USD Received 8 Oct 2013; revised 30 Dec 2013; accepted 6 Jan 2014; published 28 Jan 2014

The CCD camera registers the radiation that has passed the cell. Its spatial distribution shows interesting peculiarities that clearly demonstrate the presence of self-diffraction effects (Fig. 4). Here, results of the simulation for different cell positions are compared with the experiment. The cell position is specified by the distance $\Delta z$ between the cell central plane and the lens focal plane (see Fig. 3) and varies from $-350$ μm to 50 μm with 50 μm steps; each cell position is characterized by a group of three images numbered from (a) to (j) (see Table 2).

**Table 2. Correspondence between the cell shift with respect to the lens focus and the label of the three-image groups in Fig. 4.**

| Label in Fig. 4 | (a) | (b) | (c) | (d) | (e) | (f) | (g) | (h) | (j) |
|---|---|---|---|---|---|---|---|---|---|
| $\Delta z$, μm | –350 | –300 | –250 | –200 | –150 | –100 | –50 | 0 | 50 |
| $\eta$, $10^{-2}$ s | 0 | 4 | 7 | 8 | 9 | 0 | 12 | 15 | 0 |
| $\lvert\Delta n\rvert_{\text{mean}}$, $10^{-3}$ | 0 | 1.0 | 1.8 | 2.7 | 4.0 | 5.0 | 8.0 | 13 | 0 |

Upper images (i) present the intensity profiles in the cell plane calculated via Eq. (1). They illustrate the $I(\xi, z)$ distribution which, according to Eqs. (3) and (4), is responsible for the induced refraction index inhomogeneity. Corresponding distribution of $\Delta n$ is determined for the parameters of the disperse medium given in Table 1; afterwards, it is substituted into Eq. (2) and the distribution of the field incident onto the CCD camera is simulated (images (ii) in Fig. 4). Patterns marked (iii) show the experimental intensity distributions observed by the CCD camera. It is seen that the calculated profiles (ii) correlate adequately with the experimental distributions (iii) along the axis $\xi'$.

During the calculations, values of the coefficient $\eta$ in Eq. (3) were determined via the fitting procedure aimed at best matching the calculated plots (ii) with the corresponding sections of the measured intensity patterns (iii) of Figs. 4(b)–(h). An example of such a matching is provided by Fig. 5 where the detailed comparison between the simulation data of Fig. 4(e) (ii) and the experimental profile of the image of Fig. 4(e) (iii), taken along $y = 0$, is illustrated. The results obtained for $\eta$ due to the best fitting procedure are presented in the second row of Table 2.

#199166 - $15.00 USD Received 8 Oct 2013; revised 30 Dec 2013; accepted 6 Jan 2014; published 28 Jan 2014

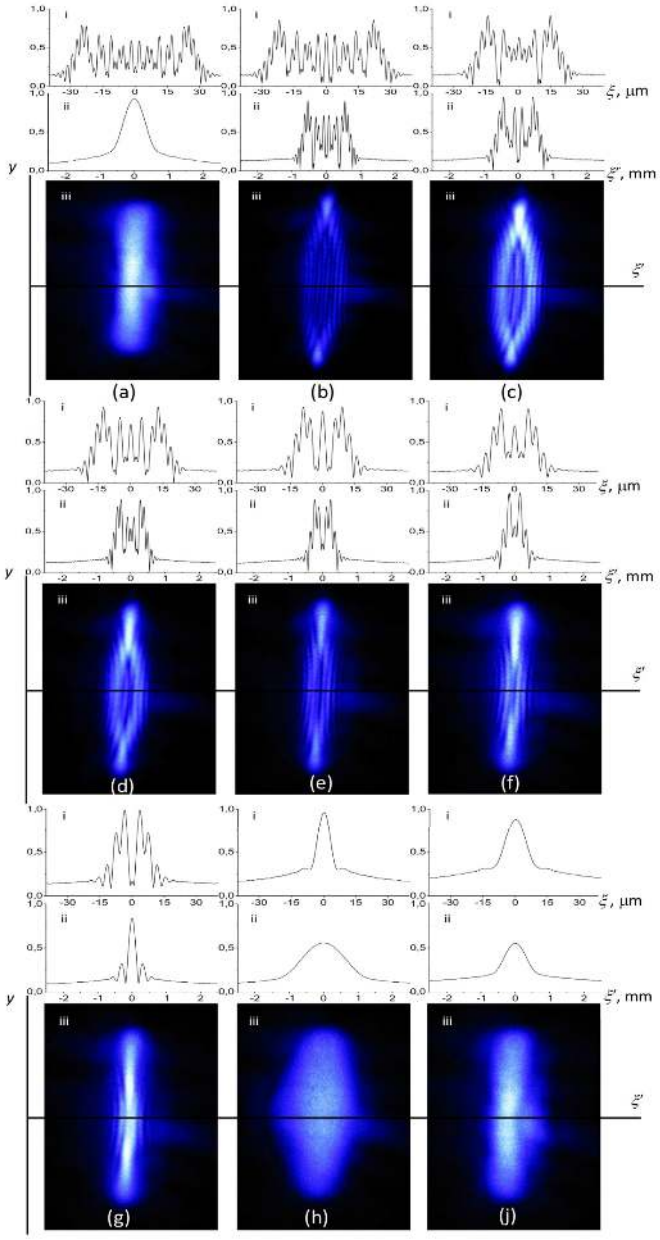


Fig. 4. Results of the numerical calculations and experimental observations of the focused beam that has passed through the disperse medium situated at different distances from the lens focus $\Delta z$; (i) calculated intensity profile in the near-focus region; (ii) calculated intensity profile behind the focus in the input plane of the CCD camera; (iii) experimentally observed intensity distributions. Groups of images (a) – (j) correspond to different $\Delta z$ (see Table 2).

#199166 - $15.00 USD Received 8 Oct 2013; revised 30 Dec 2013; accepted 6 Jan 2014; published 28 Jan 2014

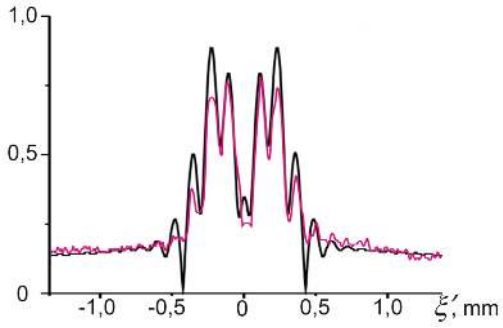


Fig. 5. Comparison of the experimental (colored curve) and theoretical (black curve) intensity distributions along $y = 0$ in the plane of observation for conditions of Fig. 4e. The black curve coincides with that of Fig. 4e (ii) and. It is obtained via Eq. (2) with allowance for Eqs. (3) and (4) and the best fitting with the experimental data has been achieved at $\eta = 9 \cdot 10^{-2}$ s (see Table 2).

Importantly, once one knows $\eta$ and the incident intensity distribution $I(\xi, z)$, the corresponding pattern of the non-linear refraction index modulation can be readily estimated along Eqs. (3) and (4). In fact, the search for adjustment between the simulated and experimental data is equivalent to the analytical calculation of $\Delta n$ in the usual Z scan method [28]. In contrast to the latter where the only measured parameter of the self-diffracted radiation was its transmission through a fixed aperture, in this work the use of modern equipment and software allows measuring the spatial distribution of the transmitted radiation in much detail and, consequently, obtaining the full pattern of the $\Delta n$ distribution rather than its single 'overall' characteristic. Leaving the detailed study of the self-induced inhomogeneity to another occasion, just for illustration, the bottom row of Table 2 supplies the mean values of the non-linear refraction index modification calculated for the mean light intensity in the cell. From the data presented one can ensure that the approach proposed enabled us to detect comparatively low non-linear modifications of the refractive index ($\sim 10^{-3}$, see Table 2) in very thin samples (the cell thickness is $d = 10$ μm). The main reason is that the fine structure of the refraction-index induced phase modulations entails perceptible structure details in the diffracted intensity distribution even if absolute phase shifts are small (in the conditions of our experiments $kd|\Delta n| < 1$).

It was experimentally revealed that when the cell was placed 350 μm before the focus (Fig. 4a) and 50 μm behind it (Fig. 4j), the presence of the medium did not influence the observed intensity distribution: the self-diffraction processes cannot develop because of the insufficient incident intensity. The corresponding distributions in Figs. 4a and 4j were visually indistinguishable from the patterns obtained when the disperse medium in the cell was replaced by pure water; exact values of $\eta$ could not be determined in those conditions and were conventionally assumed to be zero, and the non-linear refraction index variations vanished (see the first and last columns of Table 2). In all other cases (Figs. 4b–h) the patterns registered by the CCD camera represent the results of self-diffraction of the incident beam on the induced refraction index inhomogeneity following from Eq. (2).

The different values of the efficiency factor $\eta$ for different cell positions can probably be attributed to the peculiarity of the Pearcey diffraction pattern for which the characteristic size of the spatial inhomogeneity grows when moving from the lens towards the focal plane (see Fig. 2 and the patterns (i) of Fig. 4). The pre-focal transverse sections generally contain smaller details than the focal plane itself, which may slow down the thermal relaxation in the conditions of Figs. 4g, h compared to those of Figs. 4b–f. However, we could not trace this tendency forth when moving behind the focus, predominantly because of the rapid decrease of intensity and disappearance of observable non-linear effects.

#199166 - $15.00 USD Received 8 Oct 2013; revised 30 Dec 2013; accepted 6 Jan 2014; published 28 Jan 2014

When the medium is situated in the focal plane (Fig. 4h), the observed beam profile is the widest and contains no additional extrema. The fact that, in what concerns the self-diffraction efficiency, the plane (a) with $\Delta z = -350$ μm appears to be equivalent to the plane (j) with $\Delta z = 50$ μm testifies for the longitudinal asymmetry of the Pearcey pattern. Since the "geometrical" focus is blurred, the highly-inclined oblique rays leave the focal region faster, and after the focus, the beam intensity is lower than before the focus.

Both calculations and experiment have shown that in the focal plane, the incident intensity $I(\xi, f)$ is inhomogeneously distributed along the focal line (*y*-direction): the intensity is maximal near the axis and gradually decreases to the vertical edges. However, in the patterns observed behind the focus, in many cases, the intensity maxima occur near the edges (Fig. 4 b–g, iii). This is explained by the self-diffraction effects due to which the near-axis energy is redistributed between several maxima along the *x*-axis. Near the focal-line edges, the intensity is rather small and the radiation propagates in the linear regime with preserving single maximum in the *x*-direction. Note that the observed intensity distributions in the (*xy*) plane resemble the Pearcey diffraction patterns in the (*xz*) plane (see Fig. 2).

During the experiment, the laser power approximately of 100 mW (~50 mW in the cell) was maintained; with lowering the power, non-linear self-diffraction effects were rapidly suppressed, while increasing the laser power above this value led to emergence of shock waves, acoustic noise generation and eventually to the medium being destructed.

## Conclusion

Following to the way outlined before [19], we have considered additional examples of possible applications of the disperse media containing suspended absorptive micro- and nano-particles for creation of thermo-induced controllable optical switches and regulators. Carbon-coated particles suspended in water efficiently absorb and accumulate the light energy and enable articulate non-linear behavior even being exposed to comparatively weak CW laser radiation with moderate power.

In particular, in this work we present some preliminary results of theoretical and experimental studies of the self-induced laser beam transformations occurring near the focus of a cylindrical lens giving rise to the Pearcey diffraction pattern [31]. This technique can be considered as a generalization of the known Z scan method [24,25,28] enabling increase of sensitivity due to strong spatial inhomogeneity of the incident radiation. It was demonstrated that the self-focusing effect in the absorbing disperse medium takes place because of self-diffraction of the incident radiation by the phase inhomogeneity caused by the high-gradient Pearcey pattern. Due to the high intensity gradient, the self-diffraction effect occurs in very thin (micron-sized) layers; along with the small consumed power this makes the described scheme promising for integrated optical circuits.

The results obtained as well as the methods developed in this work open up new prospects in detection and measurement of weak optical nonlinearities. They testify for possibilities to observe non-linear optical effects at relatively low energy densities, i.e. in sparing conditions (note that according to the data of Tables 1 and 2, noticeable non-linear effects may occur at quite modest local heating not exceeding 10 K). This may be useful for the study of "delicate" objects, especially for biological investigations dealing with diagnostics of cells, regulation of their activity and manipulation based on the electromagnetic field interaction with matter. The media based on suspensions of strongly absorptive nanoparticles dispersed within a dielectric liquid offer additional advantages associated with the feasibility of preparation and control of the prescribed non-linear properties.

## Acknowledgments

Steen G. Hanson acknowledges the financial support from the Danish Council for Technology and Innovation under the Innovation Consortium LICQOP, grant #2416669.

#199166 - $15.00 USD Received 8 Oct 2013; revised 30 Dec 2013; accepted 6 Jan 2014; published 28 Jan 2014